Engineering Structures 98 (2015) 251–262

Contents lists available at ScienceDirect

Engineering Structures

journal homepage: www.elsevier.com/locate/engstruct

Seismic retrofitting of an HV circuit breaker using base isolation with wire ropes. Part 1: Preliminary tests and analyses

S. Alessandri, R. Giannini, F. Paolacci *, M. Malena

Roma Tre University, Rome, Italy

ARTICLE INFO

Article history:
Available online 30 March 2015

Keywords:
HV equipment
Circuit breaker
Seismic isolation
Wire rope isolators

ABSTRACT

This paper briefly describes the design and characterisation of a base isolation system that protects HV ceramic circuit breakers during seismic events. This qualifies them to the European standard CEI EN 62271-207. The solution is based on an innovative application of wire rope isolators. Preliminary numerical analyses and tests were performed on a typical HV circuit breaker and demonstrated the effectiveness of the proposed isolation system in reducing seismic demand. The results were also validated using a shaking table, which is described in an accompanying paper. The on-site installation of this system in several Italian substations has finally proved simple enough to upgrade the equipment for seismic protection.

1. Introduction

Power transmission networks are integral in modern societies. In fact, interruptions caused by seismic events may have adverse consequences on the economy and quality of life. One of the weakest parts of an electrical network is the substation, where the components are extremely exposed to seismic action. In fact, the seismic vulnerability of HV circuit breakers has recently been demonstrated by the significant damage that was observed in the aftermath of several seismic events.

For example, many circuit breakers collapsed during the Kobe earthquake, which caused several power blackouts and direct losses estimated at hundreds of millions of dollars [21]. Similar effects were recorded during the 1999 Itzmit, 1999 Chi Chi, 2003 Bahm, 2010 Christchurch and 2010 Tohoku earthquakes [11,31,16,14,20]. Based on work by Schiff [30], Anagnos [2] developed a database for electrical substation equipment performance that contains information on the damaged and undamaged components from 12 California earthquakes (from the San Fernando Earthquake in 1971 to the Northridge Earthquake in 1994). More recently, a seismic event with a magnitude of 5.8 [13] was recorded in Italy during the 2012 Emilia-Romagna earthquake; several circuit breakers collapsed, which caused service disruption and significant economic losses.

The weak resistance of this equipment against earthquakes is predominately attributed to the brittle behaviour and geometric configuration of the ceramic column, which is slender with a large mass on top [38,30,3,12,36,24,26]. In fact, brittle failures often occur at the bottom of the ceramic column, which causes the entire apparatus to collapse (Fig. 1).

The adoption of proper seismic retrofitting systems is of paramount importance. Base isolation systems have already been demonstrated to be suitable systems by several authors. Several geometric configurations of HV equipment have led to the development of various isolation systems based on friction pendulum bearings, high damping rubber bearings and wire ropes.

For example, Kircher et al. [15] investigated the dynamic properties of an ATB 7 circuit breaker mounted on GAPEC seismic isolators. As a consequence of the 1997 Bay of Plenty earthquake that caused the total destruction of a 220 kV circuit breaker, Safi et al. [29] proposed to replace the existing support stand with a base isolating tripod that uses helical springs and oil-filled dampers to control the seismic response of the circuit breaker and reduce the forces on the ceramic columns. Murota et al. [21] proposed and designed two base isolation systems for the seismic protection of electrical transformers: the first system was a combination of sliding bearings and low-damping rubber bearings, and the second was a segmented high-damping rubber bearing system (SHRB). Kong and Reinhorn [18] demonstrated the effectiveness of spherical sliding bearings (SSBs) in reducing the seismic response of disconnect switches. The use of SSBs was also investigated in a shaking test conducted by Oikonomou et al. [22] on an ABB196/230 kV bushing that was installed directly on a rigid frame.

* Corresponding author.
E-mail addresses: silvia.alessandri@uniroma3.it (S. Alessandri), renato.giannini@uniroma3.it (R. Giannini), fabrizio.paolacci@uniroma3.it (F. Paolacci), marialaura.malena@uniroma3.it (M. Malena).

http://dx.doi.org/10.1016/j.engstruct.2015.03.032
0141-0296/

Fig. 1. Collapse of a HV circuit breaker from the Emilia-Romagna earthquake (Italy).

Actually, SSBs are traditionally utilised in squat equipment or equipment with large support structures on which the ceramic columns are placed, even though wire rope isolators can also be adopted [17]. Riley et al. [28] studied the use of a friction spring damping device to reduce peak accelerations in a single pedestal support stand.

The solution based on wire ropes is particularly suitable when the period, differently from the devices traditionally utilised to protect buildings and bridges (elastomeric or SSBs), is elongated by a rocking effect rather by horizontal shear deformations [25]. They are simple devices consisting of twisted stainless steel cables wound around drilled aluminium alloy bars. The mechanical flexibility of the entire cable and the friction between the wires provide optimal mechanical isolation properties to the device in three principal directions. Wire ropes are often used for the vibrational control of industrial equipment [32]. They have never been used in practical applications as seismic isolators that have only been demonstrated in research studies [8,35,4,9,23,16,18,17]. The outcome confirmed that wire rope isolators are the suitable isolation system to mitigate the response of HV equipment to earthquakes.

The design of the base isolation system to protect HV circuit breakers against strong seismic events was commissioned by the Italian transmission system operator to Roma Tre University. This paper presents the proposed innovative solution and the analysis that was performed to demonstrate its effectiveness. The seismic qualification of the isolated apparatus has been performed through a comprehensive shaking table test, whose results are reported in a companion paper [1].

2. Analytical model of the circuit breaker

The object of this study is a pole of a 380-kV circuit breaker, which is composed of two horizontal interruption chambers placed at the top of a support element, which consists of two hollow ceramic columns connected to each other and to the chambers by metallic joints. These two columns are attached to the chambers by metallic joints. The lower ceramic column rests on a metallic box that is supported by two U200 steel girders, which are connected to each other by stiffening brackets. There are two hollow ceramic capacitors connected to the chambers. The metallic box under the ceramic column houses the operating mechanisms of the circuit breaker. An additional cabinet that contains an electric engine and other components used for the functioning of the circuit breaker is laterally connected. The arrangement of the apparatus is depicted in Fig. 2.

This circuit breaker was qualified according to CEI EN 62271-207 standard (2008) for a seismic level AF2.5.

The mechanical behaviour of the circuit breaker can be adequately described using elastic models because of the linear elastic

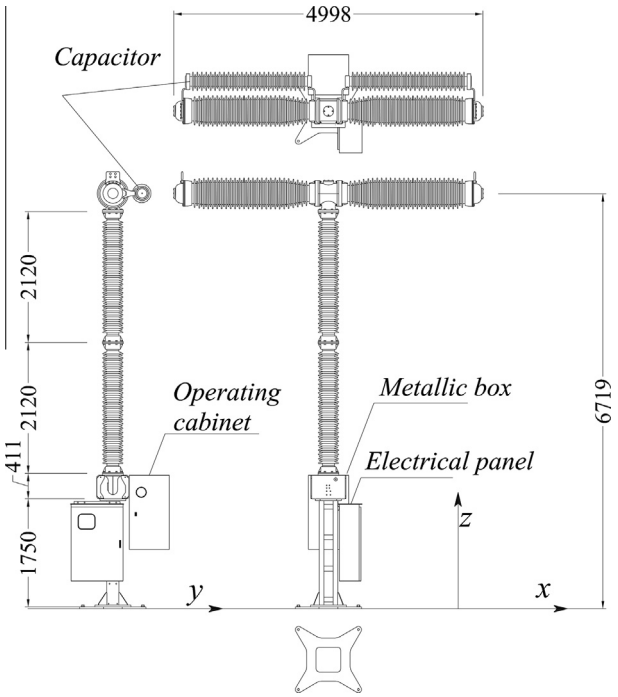

Fig. 2. Arrangement of the circuit breaker.

behaviour and the limited resistance of the ceramic columns. To assess the mechanical properties of the columns (strength and elastic modulus), of the flange joints and of the metallic box, experimental tests were performed on three different configurations: one with the column directly connected to a rigid support and the other two with the column connected to the metallic box. The ceramic columns were tested by imposing quasi-static cyclic displacement histories until to rupture. A sketch of the test setup is illustrated in Fig. 3, which also depicts the arrangement of the sensors. In this configuration the effect of the axial force generated by the superstructure has been left out. This approximation is justifiable by the preliminary character of the isolation design needed at this stage. A more precise evaluation of the mechanical characteristics was performed during a shaking table test campaign, [1].

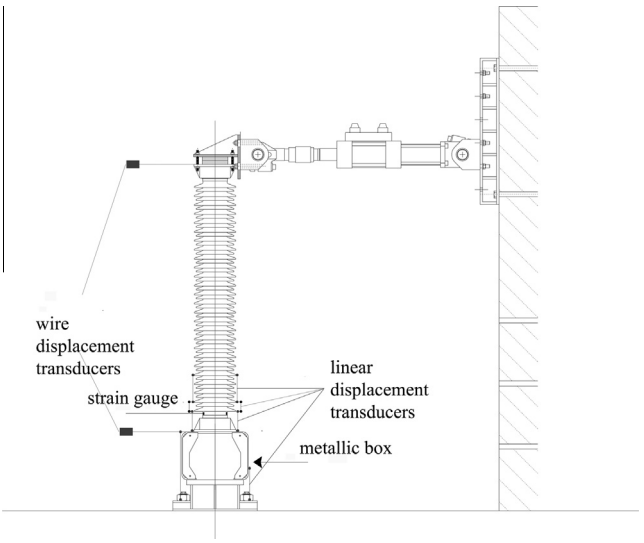

Fig. 3. Test apparatus to evaluate the mechanical properties of the ceramic column and joints.

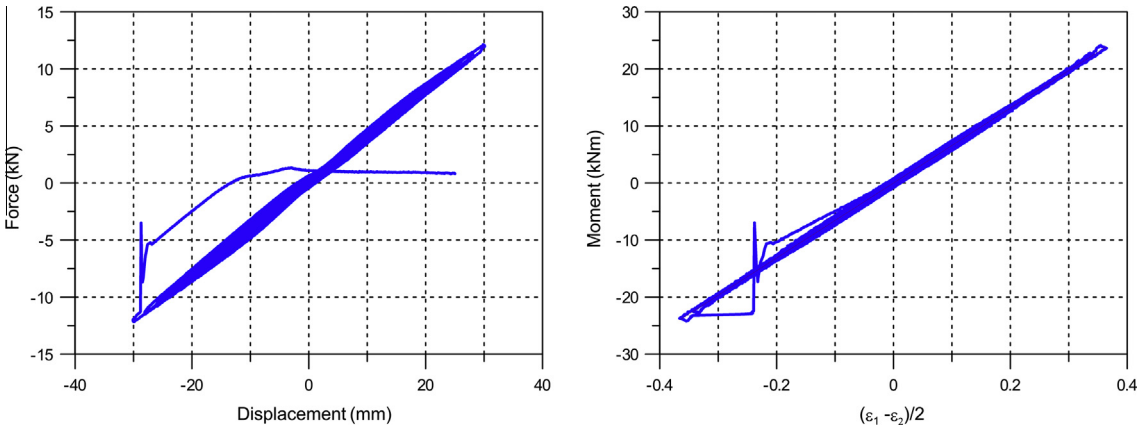

Fig. 4. Experimental force–displacement and moment–curvature cycle.

Fig. 5. Rupture in the ceramic columns.

Fig. 4 shows one of the force–deflection cycles that were obtained experimentally; the behaviour is elastic until the column base collapses (see Fig. 5). The slight hysteretic behaviour is caused by the deformability of the flange joint. The main results are listed in Table 1, where the ultimate moment (M_u), force (F_u) and strength (f_{cer}) are reported. From these results, the constant of proportionality, $K_M = 65.7$ kN m/mε, between the applied bending moment and the difference between the strains measured at the column base by the strain gauges were evaluated.

The maximum displacement at the top and the elastic modulus of the ceramic columns are also indicated in the table. The ultimate moment of the columns was almost identical in all tests and determined to be 25 kN m.

The differences between the displacements measured during the first test (column base connected to a rigid support) and those obtained during the other tests (column on the metallic box) are attributed to the high deformability of the metallic box. To evaluate the tensile strength and the elastic modulus of the ceramic, the experimental results were compared with those obtained numerically using FE Strand7 software [34]. An accurate elastic finite element model was developed that uses brick elements for the column and flange joint and shell elements for the metallic box and anchor system (see Fig. 6).

Table 1
Test results.

Test no.	F_u (kN)	h (m)	M_u (kN m)	f_{cer} (MPa)	s (mm)	E_{cer} (MPa)
1 (BF)	12.50	2.003	25.0	58.0	10.8	10^5
2	12.16	2.067	25.1	58.2	29.95	10^5
3	12.20	2.067	25.2	58.5	30.8	10^5

The difference between the experimental and numerical results is predominately attributed to the deformability of the joint (metallic box and flanged joint) that connects the column to the vertical steel support. Consequently, the stiffness of an equivalent elastic hinge was derived. The deformability of the flange joint was determined by measuring the relative displacement between the ceramic column and the metallic flange using linear displacement transducers (see Fig. 3). The estimated values reported in Table 2 were adopted to build a simplified numerical model of the circuit breaker. Elastic hinges were used to reproduce the behaviour of the joints. Elastic beam elements with equivalent area, inertia and mass density were also used to model the columns, interruption chambers, capacitors and steel supports. The additional masses of non-structural elements (e.g., cabinets) were considered as a lumped mass. The model was implemented both in Strand7 [34] and OpenSees software [19] (see Fig. 7).

The natural frequencies of the OpenSees model are listed in Table 3, where the prevailing direction of the vibration modes is also indicated (T = torsional mode around the z-axis). The first two modes are purely translational along the x and y directions, whereas the third mode is purely torsional around the z-axis.

A preliminary numerical analysis of the circuit breaker was performed using the AF5 response spectrum provided by the CEI EN 62271-207 [5], which refers to a peak ground acceleration of PGA = 0.5 g (see Fig. 8). From a standard bi-directional response spectrum analysis (100 + 30% rule) with a 2% damping ratio, a maximum bending moment of $M = 49.2$ kN m was obtained. This value is more than double the ultimate value obtained from the experimental tests, which clearly demonstrates the inadequacy of the analysed apparatus in seismic prone-zones.

3. Design of the isolation system

The high seismic vulnerability of HV circuit breakers demands the adoption of proper countermeasures. Therefore, base isolation systems are particularly effective. Well established base isolation systems are usually employed for the seismic protection of civil constructions and are based on the combination of three different phenomena: (i) elongation of the vibration period, (ii) increased damping with reduced spectral acceleration and displacement and (iii) cut-off of base shear forces transmitted to the superstructure. Elastomeric bearings (with or without lead cores) and friction pendulum predominately apply the first two phenomena, whereas elastic–plastic isolators apply the last two phenomena.

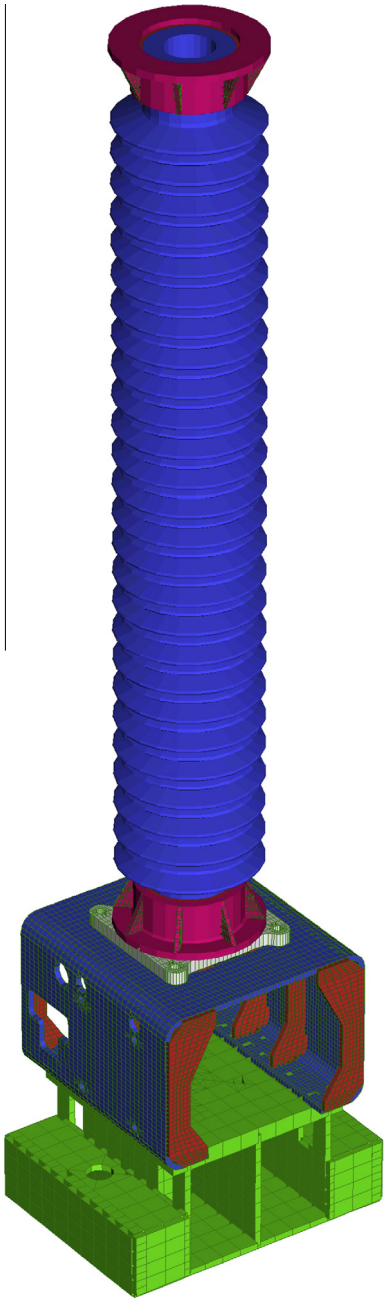

Fig. 6. Finite element model of the test specimen.

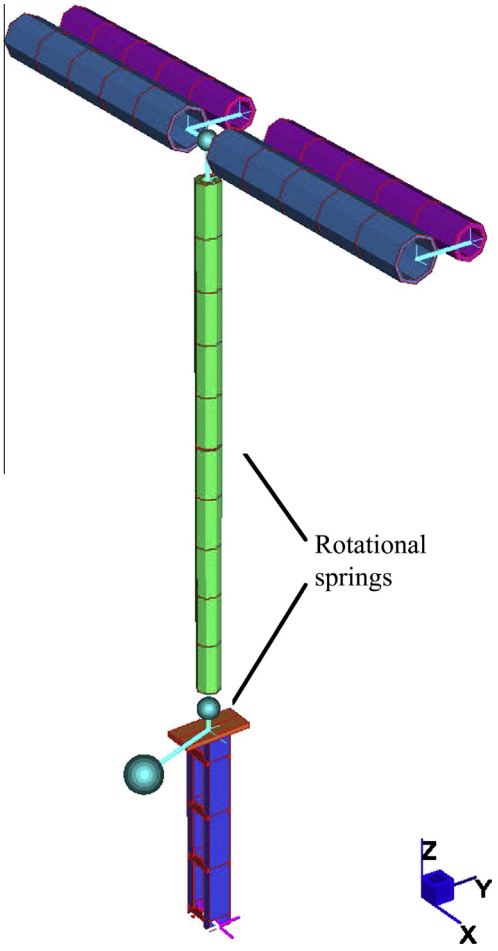

Fig. 7. Simplified FE model of the circuit breaker (Strand 7).

Table 3
Natural frequencies of the first five modes of vibration and the relevant prevailing directions of displacement.

Mode no.	Frequency (Hz)	Direction
1	0.98	*X*
2	1.02	*Y*
3	2.08	*T*
4	5.53	*X*
5	8.77	*Y*

A different solution was designed based on wire ropes, which is particularly suitable when the elongation of the period is generated by a rocking effect rather than horizontal shear deformations. The mechanical scheme of the proposed isolation system is depicted in Fig. 9. The non-linear horizontal and vertical springs simulate the vertical and horizontal behaviour of the wire rope isolators, respectively. When base rocking prevails, the vertical springs are subjected to both tension and compression forces. Because of the collapses occurred during the 2012 Emilia Earthquake a retrofitting system based on wire rope isolators has

Table 2
Stiffness of equivalent elastic hinges.

	Column on a rigid support	Column on the metallic box
K (kN mm/rad)	8.67×10^6	2.11×10^6

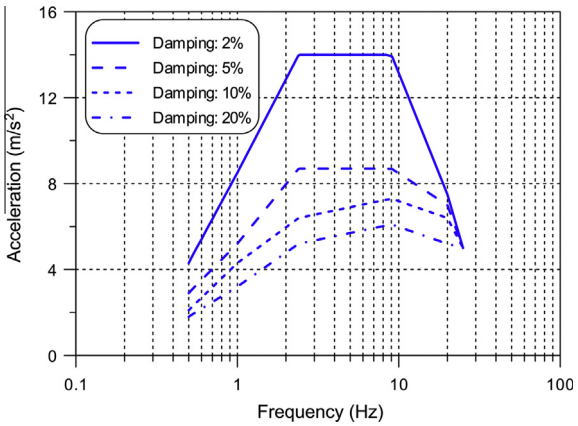

Fig. 8. CEI Standard (2008) response spectra.

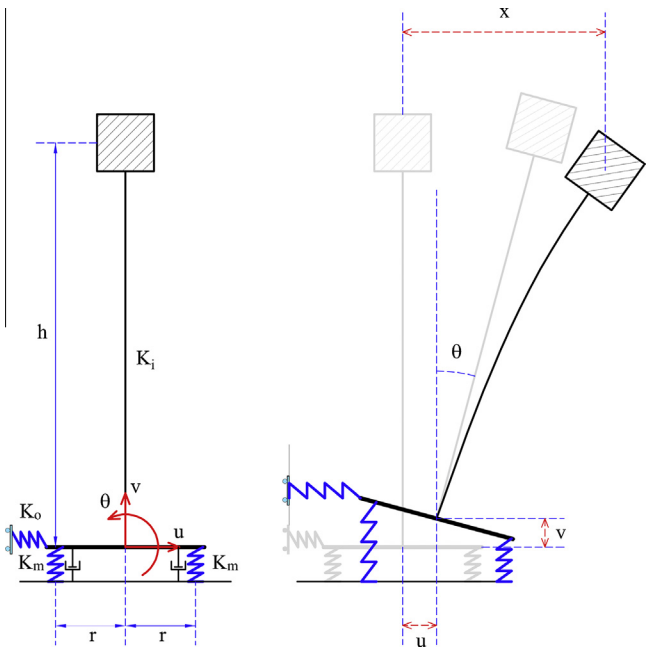

Fig. 9. Numerical model of the isolated structure.

been required by the owner to increase the seismic resistance class from AF2.5 to AF5.

3.1. Modelling the cyclic behaviour of wire ropes

Wire ropes (WRs) are simple devices composed of steel wires that are spirally wrapped and blocked by two steel bars (see Fig. 10). Their response is substantially quasi-linear elastic for horizontal deformations but significantly non-linear in tension/compression because of the geometric variation of the spires that widen in compression and tighten in tension. Consequently, a significant softening in compression and hardening in tension is observed. Additionally, friction between the wires produces significant energy dissipation, as shown by the hysteretic behaviour.

Fig. 11 shows the typical hysteretic behaviour of a WR along the principal directions: tension/compression (z), shear (x), and roll (y). The cycles are obtained by applying displacements along each direction at a time. Actually, the three responses are not entirely independent. In fact, compressive forces (z) reduced the horizontal stiffness in both the shear (x) and roll (y) directions, whereas they increased when in tension. Nevertheless, for the case study in Fig. 2, because the horizontal shear force is significantly smaller than the vertical reaction, the interaction can be neglected.

The hysteretic behaviour in shear and roll can easily be simulated using the Bouc–Wen model [37]. This model should be modified to correctly represent the strong asymmetry of the vertical response, and several authors (Demetriades et al. [8] (Schwanen [32], Paolacci and Giannini [23]) have already formulated a modified version of the Bouc–Wen model. The general constitutive equation can be written as:

$$F = f_1(x) + f_2(x)z \tag{1}$$

where $f_1(x)$ and $f_2(x)$ are functions of the displacement x and z is the internal variable of the Bouc–Wen model, solution of the following differential equation:

$$\dot{z} = A\{1 - [\beta \text{sign}(x\dot{z}) + \gamma]|z|^n\}\dot{x} \tag{2}$$

Eq. (1) generalises the equation that is commonly used to model symmetric hysteretic behaviour:

$$F = Kx + F_0 z \tag{3}$$

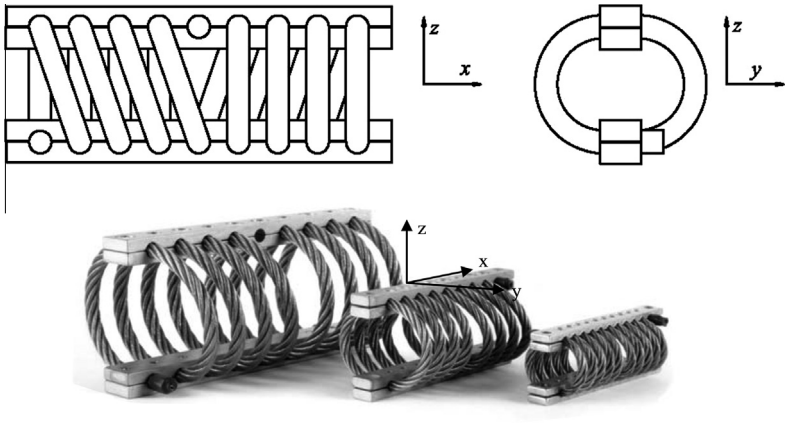

Fig. 10. Wire ropes devices (WRs).

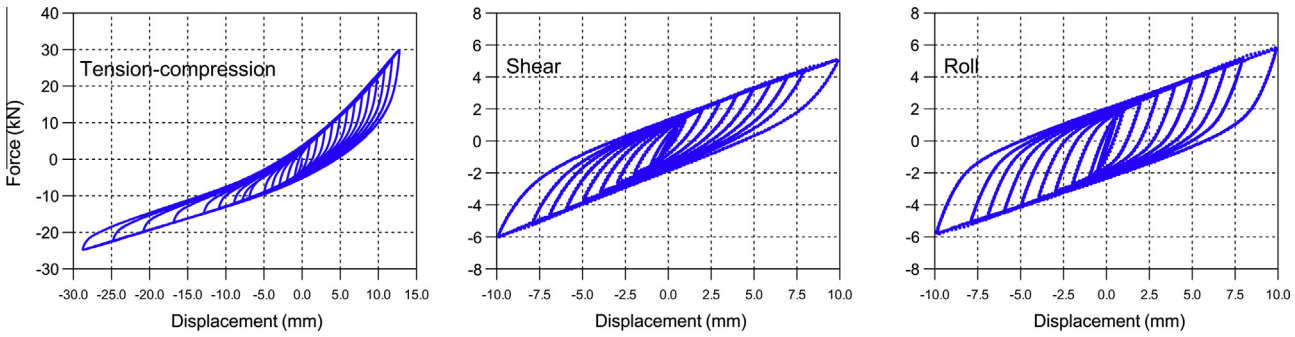

Fig. 11. Experimental force–displacement cycles along the three axial directions.

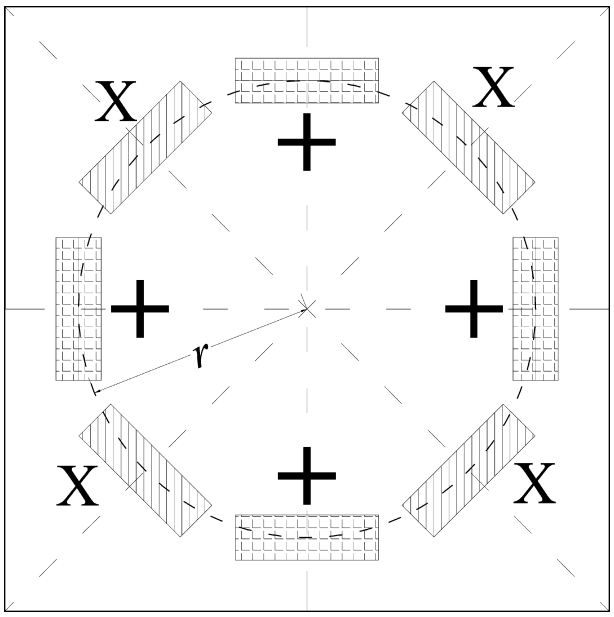

Fig. 12. Placement of wire ropes on the foundation base.

Table 4
Technical data for the wire ropes.

Model	H (mm)	W (mm)	Max static load (kN)	Max deflection (mm)
WR28-200	133	140	12.28	50.8
WR28-400	152	165	9.43	67.3
WR28-800	191	210	6.54	102.9

where K is the asymptotic stiffness and z is the variable that describe the hysteretic law. Functions $f_1(x)$ and $f_2(x)$ were used to accurately simulate the tension–compression response of a wire rope. Function $f_1(x)$ accounts for the asymptotic behaviour that is observed in tension and compression, and function $f_2(x)$ considers the varying amplitude of cycles, which are larger in tension than in compression. According to Eq. (1), a new formula was developed in this work. By assuming that the stiffness limit is K_1 when $x > 0$ and K_2 when $x < 0$, then the following can be assumed:

$$\frac{df_1}{dx} = \frac{K_1 e^{x/x_0} + K_2 e^{-x/x_0}}{e^{x/x_0} + e^{-x/x_0}} \tag{4}$$

where x_0 is a parameter that modulates the velocity of transition from K_1 to K_2. Finally, by integrating Eq. (4) we obtain:

$$f_1(x) = C + \left(\frac{K_1 - K_2}{2}\right) x_0 \log\left(\frac{1 + e^{2x/x_0}}{2}\right) + K_2 x \tag{5}$$

Function $f_2(x)$ can be generally assumed to be exponential:

$$f_2(x) = F_0 \exp\left[\left|\frac{x}{a}\right|^b \operatorname{sign}(x)\right] \tag{6}$$

3.2. Design of the isolation system

The behaviour of the isolation system depends on two parameters that control the stiffness of the entire system: the vertical stiffness (K_m) and the position (r) of the WRs. Four devices were placed on a square steel plate in two different configurations, which were designated in the following as either (X) or (+) (Fig. 12). The two configurations are substantially equivalent when the same distance from the centre (r) is used.

Wire rope isolators were selected to halve the natural frequency of the non-isolated circuit breaker. The harmonic analysis of the circuit breaker with a base acceleration $a_g = 1.0\ \text{m/s}^2$ and a damping ratio of $\zeta = 3\%$, provided the following values of base shear, bending moment and frequency for the first vibration mode:

$$V = 24.3\ \text{kN}, \quad M = 138.8\ \text{kN m}, \quad f = 0.977\ \text{Hz} \tag{7}$$

Consequently, the height of the equivalent single DOF system shown in Fig. 9 (fixed base configuration) is $h = M/V = 5.713$ m. Taking into account that at resonance the base shear is approximately given by $V = a_g m/2\zeta$ and because $a_g = 1\ \text{m/s}^2$, the mass was determined to be $m = 2V\zeta = 1458$ kg.

Neglecting the mass of the isolation system, inner damping and the translational displacements of base, the equations of motion for the isolated case can be written as follows:

$$m\ddot{x} + \frac{2K_m K_i r^2}{K_i h^2 + 2K_m r^2} x = -m a_g \tag{8}$$

where x is the relative displacement of the mass, K_m is the secant stiffness of WRs in the vertical direction, K_i is the elastic stiffness of the circuit breaker and r is the distance of the WRs from the centre of the system. From Eq. (8) we obtain:

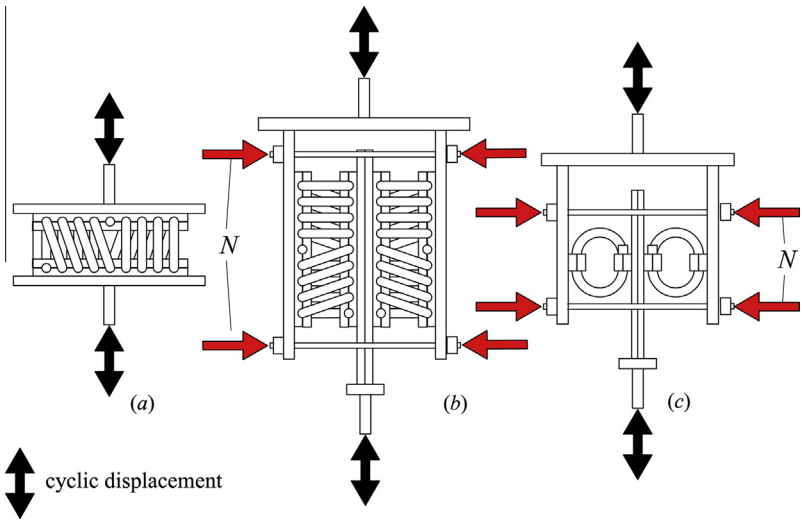

Fig. 13. Apparatus used to identify the force–displacement law for each wire rope: (a) tension–compression, (b) shear, and (c) roll.

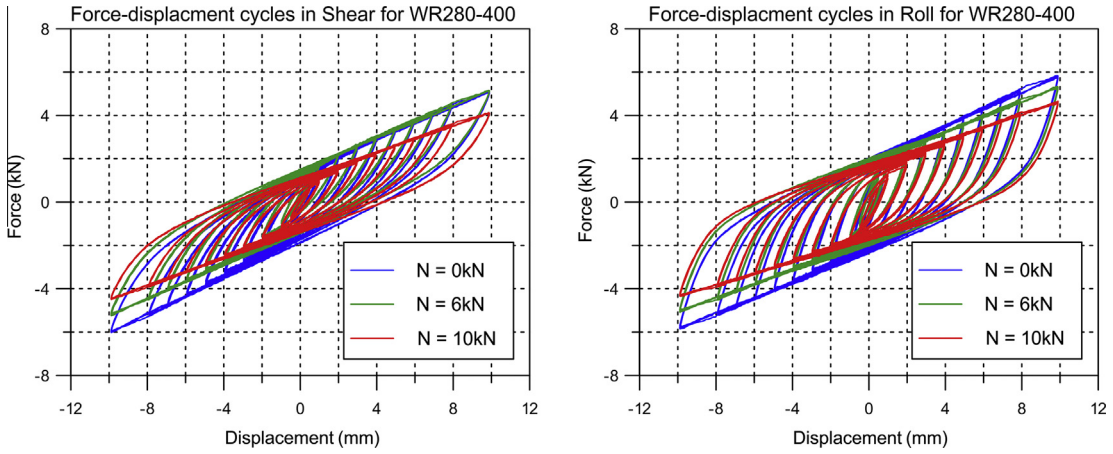

Fig. 14. Force–displacement law in shear and roll for WR280-400 at three axial force values.

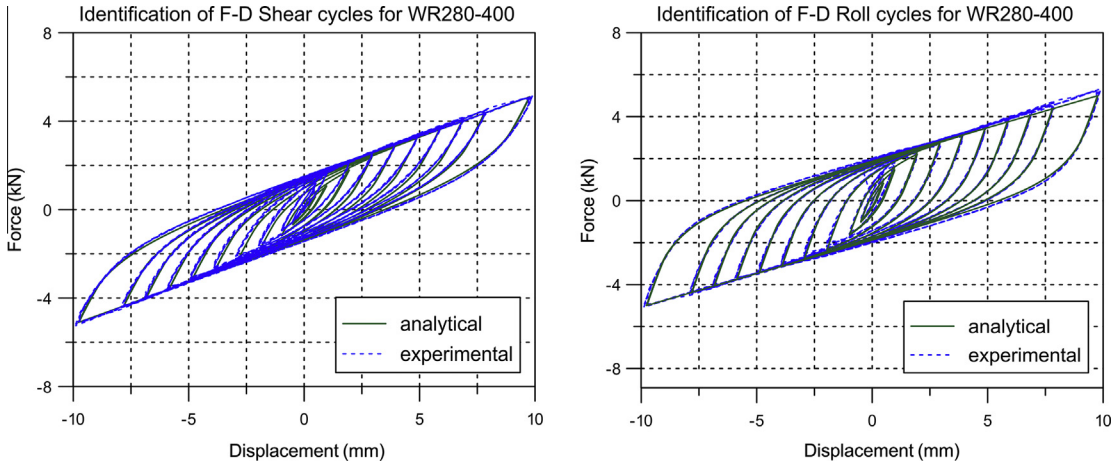

Fig. 15. Experimental and numerical responses in shear and roll for $N = 6$ kN (WR28-400).

$$\omega_{iso}^2 = \frac{2K_m r^2}{m\left(h^2 + 2\frac{K_m}{K_i} r^2\right)} \tag{9}$$

where ω_{iso} is the vibrational frequency of the isolated equipment. Finally, from Eq. (9) we obtain:

$$K_m = m\omega_{iso}^2 \frac{h^2}{2r^2\left[1 - \left(\frac{\omega_{iso}}{\omega_{bf}}\right)^2\right]} \tag{10}$$

where ω_{bf} is the natural frequency of vibration for the non-isolated system. By assuming $\omega_{iso} \approx 0.5\omega_{bf}$ and $r = 0.56$ m, we obtained $K_m = 955$ kN/m from Eq. (10). Eq. (10), although approximated, can be considered a useful tool for a preliminary design of WR isolators. The Enidine® WR28-400-08 device, which is produced in Italy (on license) by the Powerflex® Company, was selected accordingly. Stiffer and more flexible devices were also considered (WR28-200 and WR28-800), and their characteristics are listed in Table 4.

To identify the cyclic behaviour of WRs, six devices (2 for each isolator type) were subjected to cyclic displacement histories with variable amplitudes. The setup used for tension/compression, shear and roll testing is shown in Fig. 13. The variability in horizontal stiffness of the devices with gravity loads was simulated by imposing varying levels of pre-stressing forces (N) in the shear and roll testing configurations (Fig. 13b and c). The experimental cyclic response in shear and roll for WR28-400 is illustrated in Fig. 14 for various values of N. In the analysis the hysteretic law

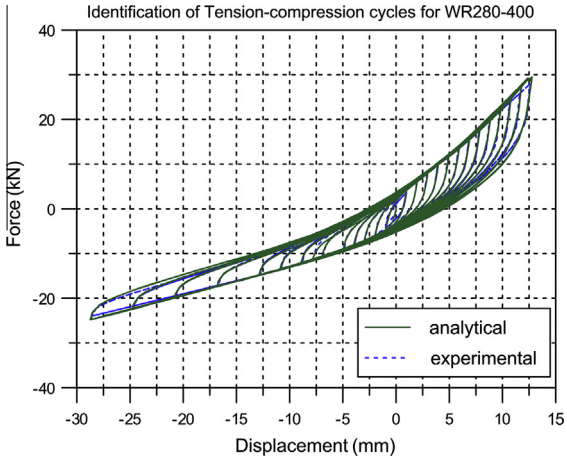

Fig. 16. Experimental and numerical responses for tension/compression (WR28-400).

corresponding to $N = 6$ kN (gravity loads) has been adopted, neglecting the interaction between vertical and horizontal hysteretic behaviour. This is justified by the limited contribution of the horizontal deformations of WRs to the global displacements (Tables 8 and 9).

These results were used to identify the parameters of the cyclic model presented in Section 3.1 (see Eqs. (1)–(5)). A Matlab©

Table 5
Parameters for tension/compression, shear and roll models (WR28-400).

	Bouc–Wen			$f_1(x)$				$f_2(x)$		
	β	γ	n	K_1 $(\frac{kN}{mm})$	K_2 $(\frac{kN}{mm})$	x_0 (mm)	C (kN)	F_0 (kN)	a (mm)	b
Shear	0.582	0.374	0.510	0.378	–	–	–	1.288	–	–
Roll	0.373	0.805	0.385	0.302	–	–	–	2.956	–	–
Tension–Comp.	1.425	−0.309	0.384	1.329	0.616	8.959	−0.588	0.190	26.919	0.751

Table 6
Configurations of the isolation system.

Type	Radius r (mm)	N	Acronym
Fixed base	–	–	FB
WR28-200	354	1	PX500
	424	2	PX600
WR28-400	300	3	M+600
	354	4	MX500
	389	5	MX550
	424	6	MX600
	537	7	MX700
WR28-800	380	8	G+760
	537	9	GX760

program was developed to determine the parameters. To simulate shear and roll behaviour, the standard formulation of the Bouc–Wen model was used assuming that $f_1(x) = K_1x$ and $f_2(x) = F_0$. In tension/compression, the model was modified according to Eqs. (5) and (6). The parameters were evaluated by minimising the mean square root of the error between the experimental and numerical results.

The numerical and experimental cyclic responses of a WR are shown in Figs. 15 and 16. The proposed model was observed to be accurate. The identified parameters for WR280-400 are listed in Table 5 ($A = 1\ mm^{-1}$).

The analytical model of the isolated circuit breaker was developed using the nonlinear FE software OpenSees [19], where a new element representing the modified Bouc–Wen model was implemented (Eqs. (1)–(6)).

3.3. Seismic response analysis

Nine different isolated configurations were analysed, each with a different wire rope typology and distance r, from the centre of the plate. These values are listed in Table 6.

The seismic response of the circuit breaker was performed using non-linear dynamic analysis. Nine triples of natural records were selected from the Pacific Earthquake Engineering Research Centre Database PEER (http://peer.berkeley.edu/products/strong_ground_motion_db.html, [27]).

Records with a magnitude of $M = 5–7$, source-site distance of $R = 5–30$ km, and soil type A were selected. An additional selection criterion was that the mean response spectrum of each component was matched as closely as possible to the CEI spectrum that was defined for a peak ground acceleration (PGA) 0.5 g and 2% damping.

All records are listed in Table 7, and the response spectra are shown in Fig. 17. Because the CEI EN 62271-207 did not distinguish vertical seismic action, the EC8 [10] spectrum was used for the definition of the vertical component of ground motion.

All records were modulated by using SeismoMatch software Seismosoft [33] to improve matching with the target spectrum and preserve several characteristics such as the non-stationary behaviour.

Table 7
Selected natural records (PEER database).

Event number	Event	Station	Year	Magnitude	Dist. (kM)	Mechanism
NGA 721	Superstition Hills-02	El Centro Imp. Co. Cent.	1987	6.54	18.2	Strike-Slip
NGA 767	Loma Prieta	Gilroy Array #3	1989	6.93	12.2	Reverse-Oblique
NGA 778	Loma Prieta	Hollister Diff. Array	1989	6.93	24.5	Reverse-Oblique
NGA 802	Loma Prieta	Saratoga – Aloha Ave	1989	6.93	7.60	Reverse-Oblique
NGA 1077	Northridge-01	Santa Monica City Hall	1994	6.69	17.3	Reverse
NGA 2374	Chi-Chi, Taiwan-04	CHY074	1999	6.20	6.00	Strike-Slip
NGA 1111	Kobe, Japan	Nishi-Akashi	1995	6.90	7.10	Strike-Slip
NGA 729	Superstition Hills-02	Wild Liquef. Array	1987	6.54	23.9	Strike-Slip
NGA 752	Loma Prieta	Capitola	1989	6.93	8.70	Reverse-Oblique

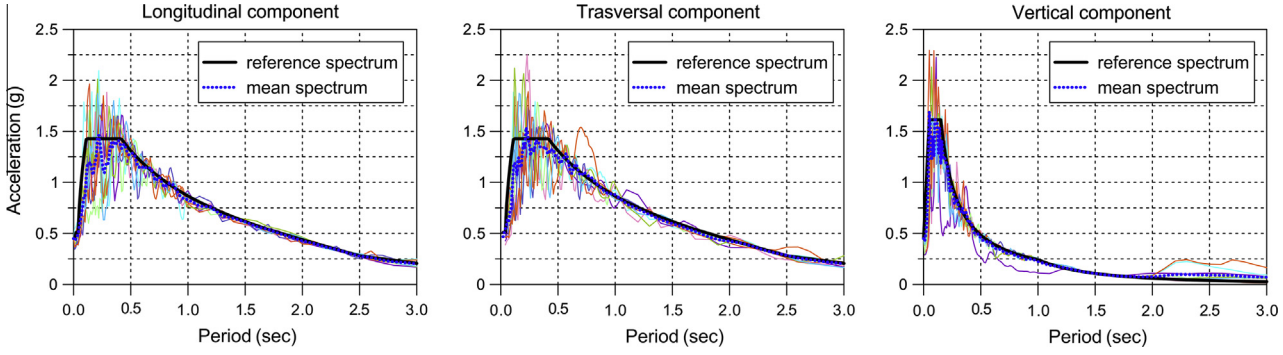

Fig. 17. Response spectra of the nine selected accelerograms and the relevant mean spectrum (dashed line) after it was matched with the reference spectrum (solid line).

A synthetic representation of the non-linear dynamic response is shown in Figs. 18 and 19. Fig. 18 shows the maximum bending moment at the bottom of the ceramic column (the most critical section of the structure) for the fixed (FB) and isolated base configurations.

Fig. 19 shows the maximum displacements along the longitudinal direction. The values are compared with those that were obtained by applying a static force of $F_w = 2.1$ kN at $z_w = 2.8$ m, which represents the maximum wind force for a velocity of 33 m/s. This velocity corresponds to the worst wind loading condition imposed by the provider to qualify the circuit breaker. These results were validated using a comprehensive shaking table test campaign; the results are discussed in a companion paper [1]. Because the vibration period of the system was longer than 2 s, the seismic displacements were barely sensitive to the system configuration. However, the wind displacements were strongly conditioned to the flexibility of the wire ropes. This suggests that the most flexible isolators (configurations GX760, M+600, and G+760) should be excluded. In fact, according to CEI EN 62271-207 (2011), a large displacement of the isolated apparatus could cause an unacceptable vertical deflection of the electrical cable that connects the equipment to adjacent structures. Therefore, the configuration that satisfies all of the requirements is the MX500, which is characterised by WR28-400 wire ropes that are placed at a distance of $r = 354$ mm, (Fig. 20). With this configuration, the mean bending moment is $\bar{M} = 13.9$ kN m and the displacement caused by wind is $S_{wx} = 120$ mm. From Fig. 18, the mean response of isolated system in terms of the bending moment is approximately the 20% of the fixed base, which demonstrates the effectiveness of wire ropes.

Mounting the isolation system is easy and fast; it requires replacing the anchorage plate, which is currently used to connect the circuit breaker to the anchor bolts of the foundation, with the isolation system. This is completed by lifting the circuit

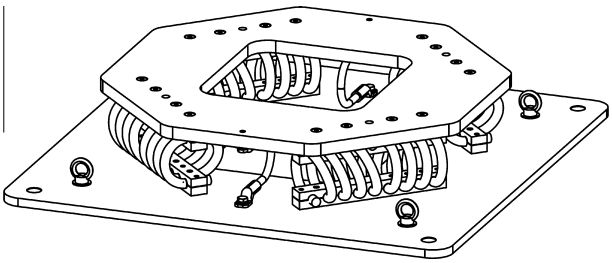

Fig. 20. Axonometric view of the isolation system.

Fig. 21. Installation of the seismic isolation system.

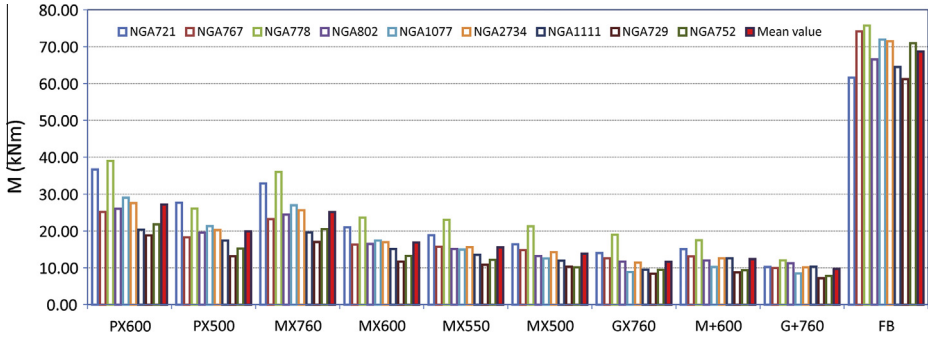

Fig. 18. Maximum bending moment at the base of the ceramic column due to seismic and wind loading.

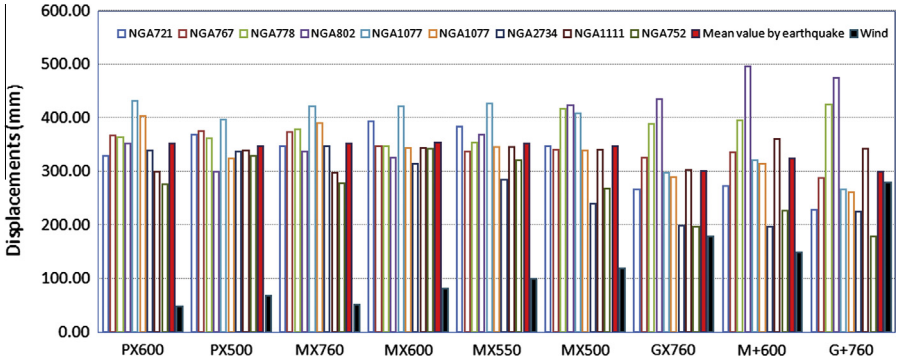

Fig. 19. Maximum displacements in the longitudinal direction seismic and wind loading.

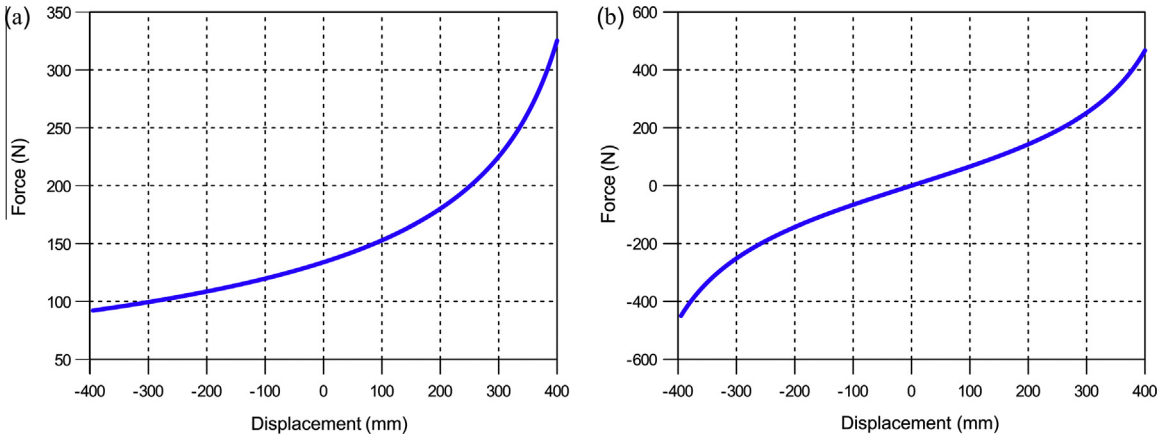

Fig. 22. Reaction force of a single cable (a) and two coupled cables acting at opposite ends (b) versus the top displacement of the isolated equipment.

breaker, disconnected from the power network and deprived of the system of internal gas, (Fig. 21). It is also necessary to replace the cable connecting the circuit breaker to the other equipment with a longer cable to avoid any dynamic interactions between the circuit breaker and the connected equipment.

3.4. Effects of the electrical connections

The analyses described in the previous section were performed while ignoring the effects of the electrical cables that connect the circuit breakers to the adjacent equipment. In the case of excessive displacement, which causes the geometric configuration of the cable to become linear, additional forces can result in the isolated equipment. For this reason, the total length of the cable must be longer than the distance between the edges of the cable.

In the present case, the length of the cable was assumed to be 500 mm greater than the distance between the two pieces of connected equipment. However, the length was limited to avoid electrical insulation problems [6]. Assuming that the motion of the isolated circuit breaker and non-isolated adjacent equipment are independent and that the maximum displacement of the latter is 170 mm [24], a relative displacement of 400 mm was obtained using the SSR combination rule.

Fig. 22(a) shows the force–displacement curve of a 7105 mm long cable with an initial distance of $l_x = 6605$ mm between the two edges and a weight density 27 kN/m; the curve was obtained by assuming a catenary deflection shape [7]. The apparatus is electrically connected by coupled cables acting at opposite ends. Consequently, the reaction force of the connection is $F_t(\delta_x) = 2[F(\delta_x) - F_t(-\delta_x)]$. The static force–deflection relationship is illustrated in Fig. 22(b). The curve is easily represented by a cubic polynomial:

$$F_t(\delta_x) = 0.566 \cdot \delta_x + 3.347 \cdot 10^{-6} \cdot \delta_x^3 \ (\mathrm{N, mm}) \tag{11}$$

where the linear term represents the initial tangent stiffness and the cubic term accounts for hardening during large displacements.

The motion of the circuit breaker is transmitted to the cables, which partially activates its mass. By assuming that the catenary shape does not change, the obtained participant mass of the cable, m_c, is 30% of the total mass of the cable (78 kg), $m_c = 23.6$ kg. The previous results show that the effect of the cable on the dynamic response of the circuit breaker is limited and therefore can be ignored. Moreover, the maximum vertical displacement of the cable is fully compatible with the requisites imposed by the European standard CEI EN 61936-1 [6] concerning the electric insulation conditions of the apparatus, expressed as minimum clearance height of the cable with respect to ground.

To validate these results, dynamic analyses were performed on isolated apparatus that added a non-linear elastic link to the top of the circuit breaker by incorporating the constitutive law given by Eq. (11) and the mass of the cable.

The response of the circuit breaker in terms of displacements and forces shows a slight difference compared with the system without the connecting cable (see Table 8). In Table 9, the maximum (positive and negative) displacements and forces of the wire ropes along the principal directions are shown. As expected, the

Table 8
Top displacements and bending moments at the column base and edges of the chambers, with and without cable connection-Central pole with the electrical control cabinet and connecting cable.

Accelerogram	Top displacements						Column base						Chambers			
	S_x (mm)		S_y (mm)		S_z (mm)		M_x (kN m)		M_y (kN m)		M (kN m)		M_x (kN m)		M_y (kN m)	
	w	w/o	w	w/o	w	w/o	w	w/o	w	w/o	w	w/o	w	w/o	w	w/o
NGA 721	335.7	314.9	327.4	326.8	10.7	10.3	12.8	12.7	12.5	12.4	16.1	16.0	5.3	5.3	5.0	5.0
NGA 767	303.4	303.9	273.5	267.9	9.2	9.1	12.3	12.4	12.2	12.5	14.9	15.0	5.1	5.1	5.3	5.3
NGA 778	296.6	304.7	450.3	450.0	11.8	11.8	16.5	16.3	14.0	13.5	17.2	17.6	5.6	5.6	4.9	4.9
NGA 802	347.2	373.3	347.9	348.0	10.4	10.5	11.0	11.9	10.2	11.4	12.4	12.6	5.1	5.0	5.3	5.3
NGA 1077	375.5	363.8	247.8	246.0	9.0	9.0	7.2	7.1	11.8	11.6	11.9	11.6	5.5	5.5	5.2	5.1
NGA 2374	314.3	311.8	253.7	253.6	7.6	7.6	10.7	10.7	10.7	11.0	12.0	12.4	5.1	5.1	6.2	6.2
NGA 1111	249.8	226.4	213.1	212.9	7.7	7.5	8.3	8.2	11.1	10.8	11.3	11.0	5.2	5.2	5.1	5.1
NGA 729	312.4	313.7	245.1	243.9	8.9	8.9	8.3	8.2	8.5	8.6	9.1	9.2	5.2	5.1	5.0	5.0
NGA 752	246.9	224.5	217.0	217.0	8.0	8.0	10.8	10.8	7.7	7.2	11.0	10.8	5.5	5.5	5.7	5.7
Mean	309.1	304.1	286.2	285.1	9.3	9.2	11.0	10.9	11.0	11	12.9	12.9	5.3	5.3	5.3	5.3
St. Dev.	42.1	48.3	76.6	72.4	1.5	1.36	2.9	2.7	2.0	1.86	2.6	2.6	0.2	0.2	0.4	0.4
CoV (%)	13.6	15.8	26.8	25.4	15.7	14.8	26.0	24.5	18.0	16.9	20.5	19.9	3.6	3.4	7.9	7.3

Table 9
Maximum displacements and forces in the WRs-Central pole with the electrical control cabinet and connecting cable.

Accelerogram	Vertical				Roll				Shear			
	S_V (mm)		F_V (kN)		S_R (mm)		F_R (kN)		S_S (mm)		F_S (kN)	
NGA 721	−30.7	9.6	−25.6	21.5	−2.4	1.3	−2.3	1.8	−1.6	0.8	−1.3	0.4
NGA 767	−24.4	6.9	−21.2	14.2	−1.4	1.7	−1.8	1.9	−1.0	1.6	−1.1	0.7
NGA 778	−35.2	11.8	−30.2	25.9	−1.8	1.0	−1.8	1.5	−1.7	1.0	−1.3	0.5
NGA 802	−29.0	8.9	−24.2	17.7	−1.2	1.3	−1.7	1.7	−1.0	1.3	−1.1	0.6
NGA 1077	−25.1	7.5	−21.7	16.1	−0.9	1.1	−1.3	1.6	−0.8	0.8	−0.8	0.5
NGA 2374	−19.6	4.7	−18.6	11.0	−1.0	1.1	−1.5	1.4	−0.9	0.9	−0.9	0.5
NGA 1111	−18.6	3.7	−18.0	8.3	−1.1	1.1	−1.5	1.4	−0.9	0.6	−1.0	0.5
NGA 729	−21.5	3.8	−19.6	9.9	−0.8	0.8	−1.2	1.3	−0.7	0.7	−0.8	0.4
NGA 752	−21.3	5.5	−19.5	12.2	−0.9	1.0	−1.4	1.4	−0.7	0.9	−0.9	0.5
Mean	−25.0	6.9	−22.1	15.2	−1.3	1.2	−1.6	1.6	−1.0	1.0	−1.0	0.5
St. Dev.	5.6	2.8	3.9	5.8	0.5	0.3	0.3	0.2	0.4	0.3	0.2	0.1
CoV(%)	22.3	40.3	17.9	37.9	41.0	24.2	20.8	12.6	35.8	32.5	19.2	16.8

shear and roll deformations were small; the average vertical displacements were within the range obtained in the experimental tests (−28 mm, 13 mm) and significantly less than the maximum value specified by the manufacturer.

4. Conclusions

This paper deals with the design of a base isolation system that retrofits a typology of HV circuit breakers for an AF5 resistance class according to CEI EN 62271-207.

The proposed system, based on wire ropes, differ from other passive devices and it is particularly suitable when the elongation of the period is generated by a rocking effect rather than by horizontal shear deformations. The mechanical flexibility of the entire cable and the friction between the wires provide the device with optimal mechanical isolation properties in all three principal directions.

To select the optimal isolation system, several configurations were numerically analysed by varying the type and position of the isolation devices. The selection of a proper device typology is a compromise between reducing the stress level in the superstructure and limiting the displacements caused by wind. In fact, excessive displacements of the electrical connecting cable in the latter can cause electrical insulation problems.

A numerical model based on the Bouc–Wen hysteretic model was specifically formulated for WRs in tension/compression and calibrated by a series of cyclic tests in displacement control for three WR typologies.

A comprehensive series of time-history analyses were performed using a non-linear model that was specially proposed for this application. The analyses demonstrated the effectiveness of this isolation systems in both serviceability and ultimate limit conditions; the displacements obtained were compatible with the electrical insulation requirements of CEI EN 61936-1, and a reduction in the bending moment by 80% was observed. These results were also confirmed through a shaking table test campaign that was performed on both the isolated and non-isolated circuit breakers. The results are described in an accompanying paper.

In conclusion, the employment of this low-cost isolation system significantly extends the life of circuit breakers, which are used in areas with medium or high seismic hazards even if the circuit breaker was are not designed to withstand strong seismic actions.

Acknowledgements

The work presented herein was supported by a financial Grant from the Italian Transmission System Operator (TERNA). Any opinions, findings and conclusions or recommendations expressed in this paper are those of the authors and do not necessarily reflect those of the funding agency. The authors thank Dr. Lorena Sguerri for the support in the execution of all experimental tests.

References

[1] Alessandri S, Giannini R, Paolacci F, Amoretti M, Freddo A. Seismic retrofitting of an HV circuit breaker using base isolation with wire ropes. Part 2: Shaking-table test validation, engineering structures; 2015. http://dx.doi.org/10.1016/j.engstruct.2015.03.031.
[2] Anagnos T. Development of an electrical substation equipment performance for evaluation of equipment fragilities. PEER Report 2001/06, April 1999; 1999.
[3] ASCE-96. Guide to improved earthquake performance of electric power systems. ASCE manual 96, American Society of Civil Engineers, Restin, VA; 1999.
[4] Bonacina G, Bonetti P et al. Seismic base isolation of gas insulated electrical substations: design, experimental and numerical activities, evaluation of the applicability. In: Duma, editor. 10th European conference on earthquake engineering; 1995.
[5] CEI EN 62271-207. High-voltage switchgear and controlgear Part 207: Seismic qualification for gas insulated switchgear assemblies for rated voltages above 52 kV; 2008.
[6] CEI EN 61936-1. Power installations exceeding 1 kV a.c. Part 1: Common rules; 2011.
[7] Dastous, Der Kiureghian. Application guide for the design of flexible and rigid bus connections between substation equipment subjected to earthquakes. PEER report 2010/4; 2010.
[8] Demetriades GF, Constantinou MC, Reinhorn AM. Study of wire rope systems for seismic protection of equipment in buildings. Eng Struct 1993;15:321–34.
[9] Di Donna M, Serino G, Giannini R. Advance earthquake protection systems for high voltage electric equipment. In: 12th European conference on earthquake engineering, London, September; 2002.
[10] EN1998-1:2005. Design of structures for earthquake resistance Part 1: General rules, seismic actions and rules for buildings. Brussels: Comit è e Europa èen de Normalisation; 2005.
[11] Erdik M. Report on 1999 Kocaeli and Düzce (Turkey) earthquakes. In: Proc of the 3rd Intl workshop on structural control, Paris – France, 6–8 July 2000; 2000. p. 149–86.
[12] Gilani AS, Chavez JW, Fenves GL, Whittaker AS. Seismic evaluation, and retrofit of 230-kV porcelain transformer bushings. PEER 1999/14 Dec. 1999; 1999.
[13] Ioannou I, Borg R, Novelli V, Melo J, Alexander D, Kongar I et al. The 29th May 2012 Emilia Romagna earthquake, EPICentre Field Observation Report No. EPI-FO-290512.
[14] Khalvati AH, Hosseini M. Seismic performance of electrical substations' equipments in bam earthquake (IRAN 2003). In: Proceedings of the 2009 Technical Council on Lifeline Earthquake Engineering conference. TCLEE. Oakland, California. June 28-July 1, 2009; 2009. p. 244–51.
[15] Kircher et al. Performance of a 230 kV ATB 7 power circuit breaker mounted on GAPEC isolators. Report by the John A. Blume Earthquake Engineering Research Center, Dept. of Civil Engrg, Stanford University, Stanford, CA; 1979.
[16] Knight B, Kempner Jr L. Seismic vulnerabilities and retrofit of high-voltage electrical substation facilities. In: Proceedings of the 2009 Technical Council on Lifeline Earthquake Engineering conference. TCLEE. Oakland, California. June 28-July 1, 2009; 2009. p. 1–12.
[17] Kong D. Evaluation and protection of high voltage electrical equipment against severe shock and vibrations. Phd dissertation, Department of Civil, Structural and Environmental Engineering, The State University of New York at Buffalo, September; 2010.
[18] Kong D, Reinhorn A. Seismic evaluation and protection of high voltage disconnect switches. In: Proceedings of the 2009 Technical Council on Lifeline

Earthquake Engineering conference. TCLEE. Oakland, California. June 28-July 1, 2009; 2009. p. 221–31.
[19] McKenna F, Fenves GL, Scott MH. OpenSees: open system for earthquake engineering simulation. Berkeley (CA): PEER, University of California; 2007. 2007.
[20] Massie A, Watson NR. Impact of the Christchurch earthquakes on the electrical power system infrastructure. NZSEE Bull 2011;44(4).
[21] Murota M, Feng MQ, Gee Y-L. Experimental and analytical studies of base isolation systems for seismic protection of power transformers, MCEER-05-0008; 2005 [30.09.05].
[22] Oikonomou K, Constantinou MC, Reinhorn AM, Yenidogan C. Seismic isolation of electrical equipment "Seismic Table Simulation". In: 15th World conference of earthquake engineering, Lisbon, Portugal, September 24–28; 2012.
[23] Paolacci F, Giannini R. Study of the effectiveness of steel cable dampers for the seismic protection of electrical equipment. In: Proceedings of the 14th world conference on earthquake engineering, Beijing, China, October; 2008.
[24] Paolacci F, Giannini R. Seismic reliability assessment of a disconnect switch using an effective fragility analysis. J Earthquake Eng 2009;13:217–35. http://dx.doi.org/10.1080/13632460802347448.
[25] Paolacci F, Giannini R, De Angelis M. Seismic response mitigation of chemical plant components by passive control systems. J Loss Prevention Process Industries 2013;26(5):879–948. http://dx.doi.org/10.1016/j.jlp.2013.03.003.
[26] Paolacci F, Giannini R, Alessandri S, De Felice G. Seismic vulnerability assessment of a high voltage disconnect switch. Soil Dyn Earthquake Eng 2014;67:198–207. http://dx.doi.org/10.1016/j.soildyn.2014.09.014.
[27] PEER strong motion database. Pacific Earthquake Engineering Research. <http://peer.berkeley.edu/smcat/> [accessed on January 2012].
[28] Riley M, Stark C, Kempner Jr L, Mueller W. Seismic retrofit using spring damper devices on high-voltage equipment stands. Earthquake Spectra: August 2006 2006;22(3):733–53.
[29] Safi BF, Pham LT, Busby MJ. High voltage circuit breaker supported on a base isolating tripod for earthquake protection. In: IPENZ annual conference 1990, proceedings of: engineering, past, present and future: building the environment; volume 1: civil; 1990.
[30] Schiff AJ. Earthquake effects on electric power systems. ASCE J Power Div 1973;99(2):317–28.
[31] Shiff AJ, Tang AK. Chi-Chi, Taiwan, earthquake of September 21, 1999: lifeline performance, Technical Council of Earthquake Engineering, ASCE, Monograph no. 18, July; 2000.
[32] Schwanen W. Modelling and identification of the dynamic behavior of a wire rope spring. Technische Universiteit Eindhoven, The Netherlands, Report number: DCT-2004/28, Master Thesis, 2004; 2004.
[33] Seismosoft. SeismoMatch v2.1 – a computer program for spectrum matching of earthquake records; 2013. <http://www.seismosoft.com>.
[34] Strand 7 Pty Ltd. Introduction to the Strand 7 finite element analysis system. 3rd Ed.; 2010. <www.strand7.com> [viewed by authors April 2014].
[35] Serino G, Bonacina G, Bettinali F. Passive protection devices for high-voltage equipment: design procedures and performance evaluation. In: Proceedings of the fourth U.S. conference sponsored by the Technical Council on Lifeline Earthquake Engineering/ASCE.Strand 7 "Finite Element Analysis System. User Manual" Strand7 Pty Ltd. (2010); 1995.
[36] Takhirov SM, Gilani ASJ. Earthquake performance of high voltage electric components and new standards for seismic qualifications. In: Proceedings of the 2009 Technical Council on Lifeline Earthquake Engineering conference. TCLEE. Oakland, California. June 28-July 1, 2009; 2009. p. 274–84.
[37] Wen Y. Method for random vibration of hysteretic systems. J Eng Mech Div, Proc ASCE 1976;102(2):249–63.
[38] Winthrop DA, Hitchcock HC. Earthquake design of structures with brittle members and heavy artificial damping by the method of direct integration. Bull NZ Soc Earthquake Eng 1971;4(2).